# HOST GALAXIES OF QUASARS AND THEIR ASSOCIATION WITH GALAXY CLUSTERS

T. GEHREN, 1,2 AND J. FRIED Max-Planck-Institut für Astronomie, Heidelberg

AND

P. A. WEHINGER<sup>1</sup> AND S. WYCKOFF Department of Physics, Arizona State University Received 1983 May 10; accepted 1983 August 19

#### **ABSTRACT**

Seventeen quasars with redshifts ranging from 0.044 to 0.828 have been observed through an r filter using a CCD detector at the Cassegrain focus of the Max-Planck-Institut für Astronomie 2.2 m telescope. A surface brightness detection limit of 26 mag arcsec<sup>-2</sup> for the highest quality images was attained. Using a point-spread function defined by field stars exposed on the same CCD frame as the quasar, point-by-point subtraction of the quasar nucleus from the image reveals some of the structure in the nebulosity underlying essentially all quasars with redshifts  $\lesssim 0.5$ .

Under the assumption that the quasar nuclei and the underlying nebulosities have the same cosmological redshifts, absolute magnitudes and metric diameters of the resolved structures again support the interpretation that quasars are central events in distant *galaxies*. While underlying galaxies of radio-loud quasars may occupy a wide range in luminosities, their average absolute magnitude is  $\langle M_r \rangle = -22.8 \pm 0.7$ . There is some evidence that host galaxies of radio-quiet quasars may on average be 2 mag fainter than those of radio-loud quasars. Moreover, the average metric diameter of radio quasars,  $\langle D \rangle = 128 \pm 34$  kpc, may be significantly greater than that observed for radio-quiet quasars, for which we find  $\langle D \rangle = 37 \pm 8$  kpc. Intensity profiles of the resolved underlying nebulosities can be fitted by a *power law* with log  $I(r) = \alpha \log r + \text{const}$ , where  $\alpha = -1.96 \pm 0.36$  is essentially the exponent expected for a Hubble-type intensity law. The correlation between the luminosity of the quasar nucleus and that of its host galaxy indicates that the luminosity of the nucleus occupies approximately the same magnitude range as the underlying galaxy. The morphologies of the resolved galaxies underlying the quasars PHL 909, 3CR 48, and 0241+622 are suggestive of tidal interactions with nearby companion galaxies.

Counts of faint galaxies in the vicinity of the quasar images indicate that quasars are usually situated in groups or *clusters of galaxies* which are dominated by the luminosity contribution of the quasar host galaxy. We conclude that most of the radio quasars are central events in galaxies which are more luminous and larger on average than normal elliptical and spiral galaxies. We suggest that most radio-loud quasars are in giant elliptical galaxies in which a considerable amount of hot gas and young stars may be present due to recent collisions or tidal interaction with nearby cluster members.

Subject headings: galaxies: clustering — galaxies: nuclei — galaxies: photometry — galaxies: structure — quasars

# I. INTRODUCTION

Recent studies of Wyckoff, Wehinger, and Gehren (1981) and Hutchings et al. (1981, 1982) have shown that the majority of low-redshift quasars are surrounded by extended nebulosities, as originally suggested by Matthews and Sandage (1963) and others (cf. Arp 1970; Gunn 1971; Kristian 1973; Hawkins 1978). However, the quantitative properties of underlying nebulosities are not yet firmly established. Due to the lack of statistical significance of the small sample of quasars observed to date, and to different methods of data reduction, large-scale sky-limited photometry of quasars has led to slightly different interpretations of the properties of the extended nebulosities underlying the low-redshift quasar images. Both Wyckoff, Wehinger, and Gehren (1981) and

Hutchings et al. (1981, 1982) agree that the properties of the nebulosities are consistent with those of galaxies. However, Hutchings et al. (1982) derived absolute magnitudes of the underlying galaxies that are 0.5–1.0 brighter than those of Wyckoff et al., with no differences in the absolute magnitudes between radio-loud and radio-quiet quasars. Hutchings et al. (1982) have also claimed that the intensity profiles of the underlying nebulosities can be better fitted with an exponential than a power law; while the radially averaged profiles of Wyckoff et al. conform better to a power law. Both groups have found that the underlying galaxies are less luminous than are the brightest members of clusters.

Following several marginal detections of absorption lines in spectra of nebulosities underlying quasars (Wampler et al. 1975; Stockton 1976; Richstone and Oke 1977; Wyckoff et al. 1980a, b; Miller, French, and Hawley 1980; Miller 1981), recent observations (Boroson and Oke 1982; Boroson, Oke, and Green 1982) have established beyond doubt absorption

<sup>&</sup>lt;sup>1</sup> Visiting Astronomer, German-Spanish Astronomical Center, Calar Alto, operated by the Max-Planck-Institut für Astronomie, Heidelberg, jointly with the Spanish National Commision for Astronomy.

<sup>&</sup>lt;sup>2</sup> Now at Universitäts-Sternwarte München.

lines present in quasar fuzz. In fact Boroson and Oke (1982) conclude that 3CR 48 is centered in a giant spiral galaxy with a luminosity corresponding to  $M_v = -23$  or brighter, while Boroson, Oke, and Green (1982) find that the luminosities of the galaxies underlying radio-quiet quasars are on the average 1-2 mag fainter than those of the brightest cluster galaxies. Thus both the photometric and spectroscopic observations of quasar nebulosities seem to favor the hypothesis that quasars reside in host galaxies that are significantly fainter than first-ranked giant elliptical galaxies. That such host galaxies tend to be of spiral type has been found by Boroson, Oke, and Green (1982) and Hutchings et al. (1981, 1982). On the other hand, some underlying galaxies like those of 3CR 48 (Boroson and Oke 1982) or 3CR 273 (Wyckoff, Wehinger, and Gehren 1981) may be much more luminous. While spectroscopic confirmation of the galaxy nature of the underlying nebulosity is certainly necessary, photometric imaging may be used to determine reliable integrated data, which serve to derive important statistical properties of quasar galaxies.

In this paper we report new imaging results obtained with the CCD camera recently installed at the Max-Planck-Institut für Astronomie (MPIA) 2.2 m telescope. The observations, reduced with newly developed two-dimensional software, are described in § II, while the results are presented in § III. In § IV we discuss our measurements of faint galaxies found near quasars. Section V contains the discussion of the results: the luminosity distribution of the host galaxies, their morphologies and possible interaction with nearby companion galaxies.

### II. OBSERVATIONS AND DATA REDUCTION

Our present sample  $(z \le 0.6)$  was taken from the QSO catalog of Hewitt and Burbidge (1980) and consists of 13 radio-loud and three radio-quiet quasars. As a control, one object (4C 19.34) with z = 0.828 was included in the observing program.

The observations were made in 1982 March and October using an RCA CCD array with  $512 \times 320$  pixels at the Cassegrain focus of the MPIA 2.2 m telescope at the Calar Alto Observatory in southern Spain. The focal plane image scale is 0".34 per 30  $\mu$ m channel width. The detector was cooled with liquid nitrogen to 150 K. Because of the small field of the detector  $(2' \times 3')$  the frames were carefully positioned in order to record simultaneously the images of the quasar and at least one star of similar magnitude to define the combined atmospheric plus instrumental point spread function. All images were exposed for 60 minutes through an r filter (cf. Thuan and Gunn 1976). The magnitude calibration was tied to observations of Thuan and Gunn's primary standard subdwarf BD +17°4708, and the basic observational data are given in Table 1.

The first step in the data reduction consisted of flat field correction and removal of hot pixels. The flat field was constructed in the following way: from each object frame we removed all outstanding features (e.g., stars and galaxies) by interactively marking a window centered on the feature and replacing all pixels in the window by the average of all pixels on the rim. The final flat field was obtained by co-adding all frames processed in this way. After flat field correction, the global variations in the sky background were

TABLE 1 JOURNAL OF OBSERVATIONS

QSO	Name	Type <sup>a</sup>	z	$m_v^{\ b}$	$m_r^{c}$	$\mu_r^{\mathrm{d}}$	se
1. 0003 + 158	PHL 658	R	0.450	16.40	16.03	20.72	1.7
2. $0043 + 388 \dots$	*	O	0.189	18.39	19.18	20.72	2.7:
3. $0054 + 144 \dots$	PHL 909	R	0.171	16.70	15.75	20.70	2.1
$4. \ 0134 + 329 \dots$	3CR 48	R	0.367	16.20	15.97	20.79	2.0
$5. 0154 + 316 \dots$	4C 31.06	R	0.373	18.90	18.27	20.81	2.7
6. $0214 + 108 \dots$	4C 10.06	R	0.408	17.00	16.69	20.77	1.8
7. $0241 + 622 \dots$		R	0.044	15.70	16.08	20.59	2.1:
8. $0429 + 415 \dots$	3CR 119	R	0.408	20.00		20.68	2.0
9. $1022 + 194 \dots$	4C 19.34	R	0.828	17.49	17.20	20.33	1.4
10. $1257 + 286 \dots$	X Com	O	0.092	17.50	16.64	20.65	1.3
11. 2130 + 099	II Zw 136	O	0.061	14.64	14.76	20.57	2.1
12. $2141 + 175 \dots$	OX 169	R	0.213	15.50	16.29	20.52	2.5
13. $2201 + 315 \dots$	4C 31.63	R	0.297	15.47	15.54	20.59	1.9
14. $2214 + 350 \dots$		R	0.510	18.50	18.25	20.39	2.4
15. 2247 + 140	4C 14.82	R	0.237	17.00	16.74	20.92	2.0
16. 2252 + 129	3CR 455	R	0.543	19.70	18.79	20.40	2.6
17. 2308 + 098	4C 09.72	R	0.432	15.00	16.15	20.60	1.6

<sup>a</sup> R = radio-loud, O = radio-quiet.

<sup>b</sup> V magnitude from Hewitt and Burbidge 1980.

<sup>c</sup> Calibrated r magnitude.

<sup>d</sup> r bandpass night-sky brightness in mag arcsec<sup>-2</sup>.

e FWHM seeing disk in arcsec, colon denotes bad guiding.

always smaller than the background noise. Most important, this method of flat field correction removed the pattern of interference fringes which are produced in the thin layer covering the CCD. The amplitude of these fringes, originally at the 1% level, is reduced by an order of magnitude, and therefore our data analysis is not affected by the interference problem. It should be emphasized here that this flat field procedure is only applicable if the temperature of the CCD is stabilized within  $\sim 0.2$  K, since the amplitude and position of the fringes depend critically on the temperature stability of the CCD chip. The high stability of our Dewar system  $(\pm 0.1 \text{ K})$  allowed the use of all frames obtained during the observing runs to compose the flat field.

There are at least two more sources of image degradation in addition to the expected flat field effects (i.e., pixel-to-pixel variations and global changes of mean sensitivity): the first one concerns hot and cold pixels, which have been removed by applying a median filter. This yields reasonable corrections as long as such CCD defects are not centered on a point source image where the intrinsic gradients are of the same order as those of hot pixels, thus making discrimination between the real signal and the CCD defect impossible.

Whereas cosmetic defects such as interference fringes and hot or cold pixels could very well be corrected, the second source of image degradation could not be removed: radial fringes centered on each point source. Their radial maxima are roughly equally spaced. Possible explanations are internal multiple reflections on the optical surfaces and/or beat frequencies resulting from diffraction at both the outer (primary diameter) and inner (secondary cover) edges of the telescope aperture. Therefore, the local sky background as determined from carefully selected windows in each CCD frame may be in error by as much as  $\sim 0.3\%$ , currently limiting our photometric accuracy to about 6 mag below the night sky. This limit is not a result of the CCD noise but of poorly understood image degradation. It is clearly visible in the profiles of faint quasars such as 0043 + 388, 0154 + 316, 2214 + 350, and 2252 + 129, and it is also seen in the photographic images obtained with a different telescope (cf. Wyckoff, Wehinger, and Gehren 1981).

As a second step in our data reduction procedure we computed integrated magnitudes and surface brightness profiles. This software is an extension of the one used for the interpretation of photometric data (cf. Wehinger, Gehren, and Wyckoff 1980), with the following improvements: (1) The magnitude calibration is no longer derived from the uncertain (and sometimes variable) V magnitude of the quasars. Instead of assuming  $V_{QSO} = F_{QSO}$ , where F is the photographic bandpass defined by the combination of the IIIa-F emulsion +OG 570 filter, the CCD r magnitudes are directly related to measurements of the standard star BD  $+17^{\circ}4708$ . (2) Since the CCD images obtained for the current sample of quasars are not saturated near the image centers, a desaturation procedure proved unnecessary. (3) Due to the large dynamic range of the detector, the point-spread function (PSF) is in most cases defined by a single star. (4) The detection of underlying nebulosity is based on a point-by-point subtraction of the appropriately scaled PSF from the quasar image, for which a careful determination of the centers of the PSF and the QSO image is necessary. The appropriate scaling factor for the PSF is determined by trial and error such that (a) the resulting difference image is nonnegative, and (b) the azimuthally averaged intensity profile of the difference image is the minimum of all possible profiles increasing monotonically toward the center of the image. Although conditions (a) and (b) do not guarantee a unique result, they provide a realistic estimate of the lower limit of the underlying galaxy's luminosity. Ideally, condition (b) should lead to a difference image with no point-source component in the center. It was found that a variation of the scaling factor within reasonable limits does not affect the low-luminosity structure of the underlying galaxy. However, the residual surface brightness of the underlying galaxies is uncertain near the center, sometimes resulting in artificial structure within the inner 1" or 2". Such defects are due to hot or cold pixels that survived the cleaning of the raw CCD images. We have omitted all secondary objects (field stars or companion galaxies) while sampling the azimuthally averaged intensity profiles or the integrated magnitudes.

In the discussion which follows we shall refer to the observed nebulosities underlying the quasars as host galaxies and assume that they are physically associated with the quasar nuclei. Though our data have not been obtained under perfect observing conditions, it seems useful to compare our present results with those obtained using hypersensitized IIIa-F plates combined with an OG 570 filter in the prime focus of a 3.6 m telescope. At least four important advantages should be noted: (a) the linearity of the CCD allows a photometric calibration with respect to standard stars, (b) saturation in the centers of quasar and stellar images presents a minor problem because of the large dynamic range of the CCD, (c) problems connected with the microdensitometer scanning of photographic plates are avoided, and (d) under equivalent observing conditions the high detective efficiency of the CCD leads to the detection of fainter structure. Whereas (a) and (b) contribute strongly to the reduction of systematic errors entering the photometric results, the fivefold to tenfold increase in the signal-to-noise ratio yields an improvement in surface brightness levels of at least 1-2 mag arcsec<sup>-2</sup> as compared with photographic plates.

#### III. IMAGING RESULTS

Isophotal maps and azimuthally averaged intensity profiles are presented in Figure 1, which shows the well-resolved quasars. Figure 2 displays isophotal maps of those quasars that either are poorly resolved (0003+158, 1022+194, and 2308+098) or for which the image of the underlying galaxy contained no obvious structural information. An isophotal map of the quasar 0429+415 (3CR 119) is not shown because it is blended heavily with a star 1".5 to the northeast, and the image could not be reduced with our current techniques. Notes on the individual objects are given in § IIId.

Comparison of the quasar images with the point-spread functions in Figures 1 and 2 shows immediately that virtually all quasars are resolved at low light levels (24–26 mag arcsec<sup>-2</sup>).

### a) Absolute Magnitudes and Metric Diameters

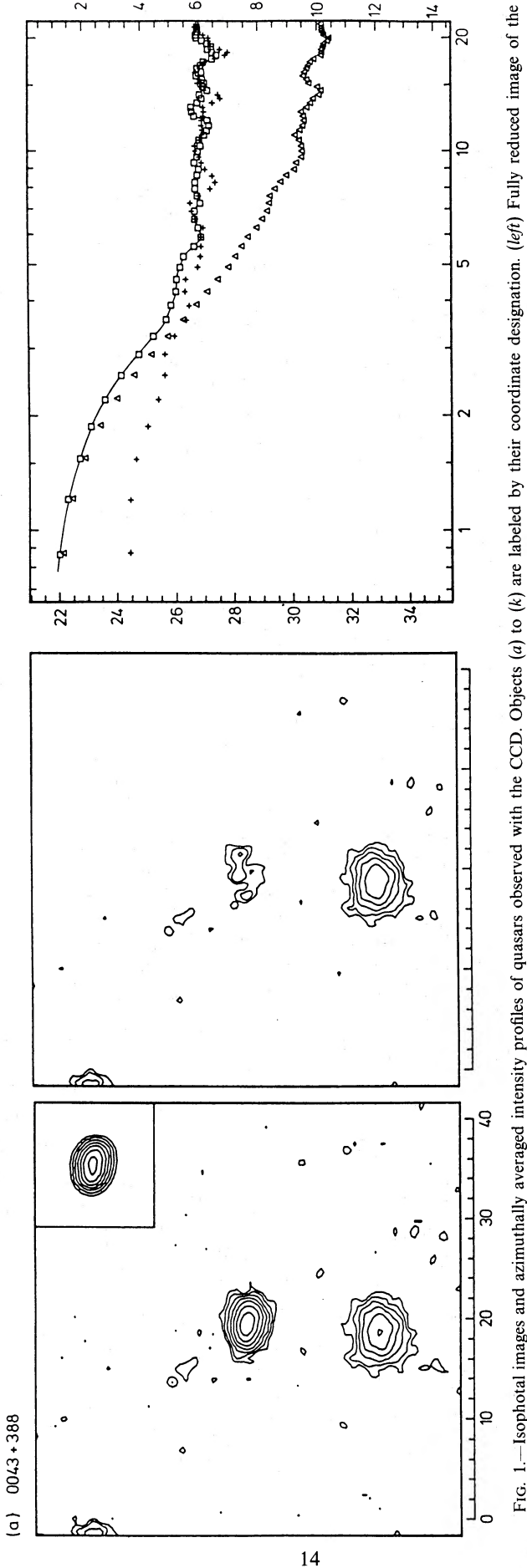
Integrated apparent r magnitudes have been obtained by sampling the intensities of the underlying galaxies in an area as large as possible, in all cases exceeding the radial distances at which the surface brightness falls below  $\mu_r = 26$ mag arcsec<sup>-2</sup>. Since the concept of a standard metric diameter is premature for the host galaxies of quasars, no aperture corrections were applied. The resulting integrated magnitudes of the underlying nebulosities are given in column (4) of Table 2. There are essentially two sources of systematic errors in the photometry: (1) The determination of the sky background is uncertain either because of the residual fringes in the image (cf. § II), or because of locally increased background from nearby objects (1257+286, 2214+350, and 2252+129). (2) Host galaxy magnitudes of quasars near the limit of resolution are uncertain, because the integrated magnitudes rely essentially on difference structure near the image centers which sometimes is not reliable. We estimate the combined errors in the photometry to be less than 0.5 mag, except for 0043+388 and 2214+350, where a systematic error of more than 0.5 mag cannot be ruled out.

Isophotal angular diameters  $\theta$  have been determined from azimuthally averaged image profiles at the surface brightness levels of  $\mu_r = 26$  mag arcsec<sup>-2</sup>. They do not represent the maximum extensions of the host galaxies. In a few cases these diameters are uncertain, as indicated by colons in Table 2, and for 0003 + 158 and 1022 + 194 we give only upper limits.

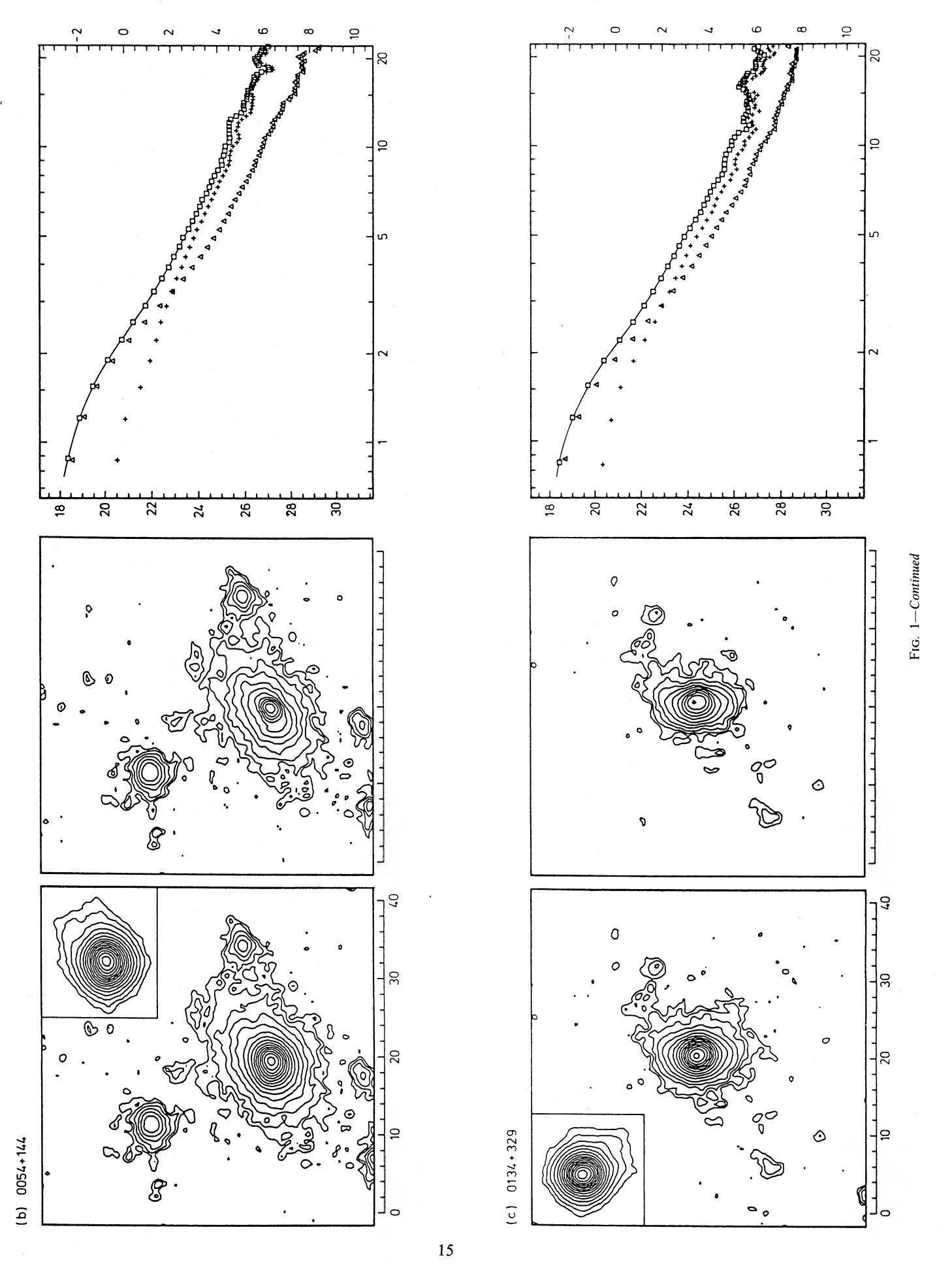
The determination of absolute magnitudes and metric diameters of the galaxies underlying the quasars involves corrections for galactic extinction and bandpass shift (K-correction) due to the assumed recessional velocities of the associated quasars. Mean values of interstellar reddening as a function of galactic latitude, given by Sandage and Visvanathan (1978), yield approximately

$$A_r \approx 0.075 (\operatorname{cosec} |b| - 1)$$
,

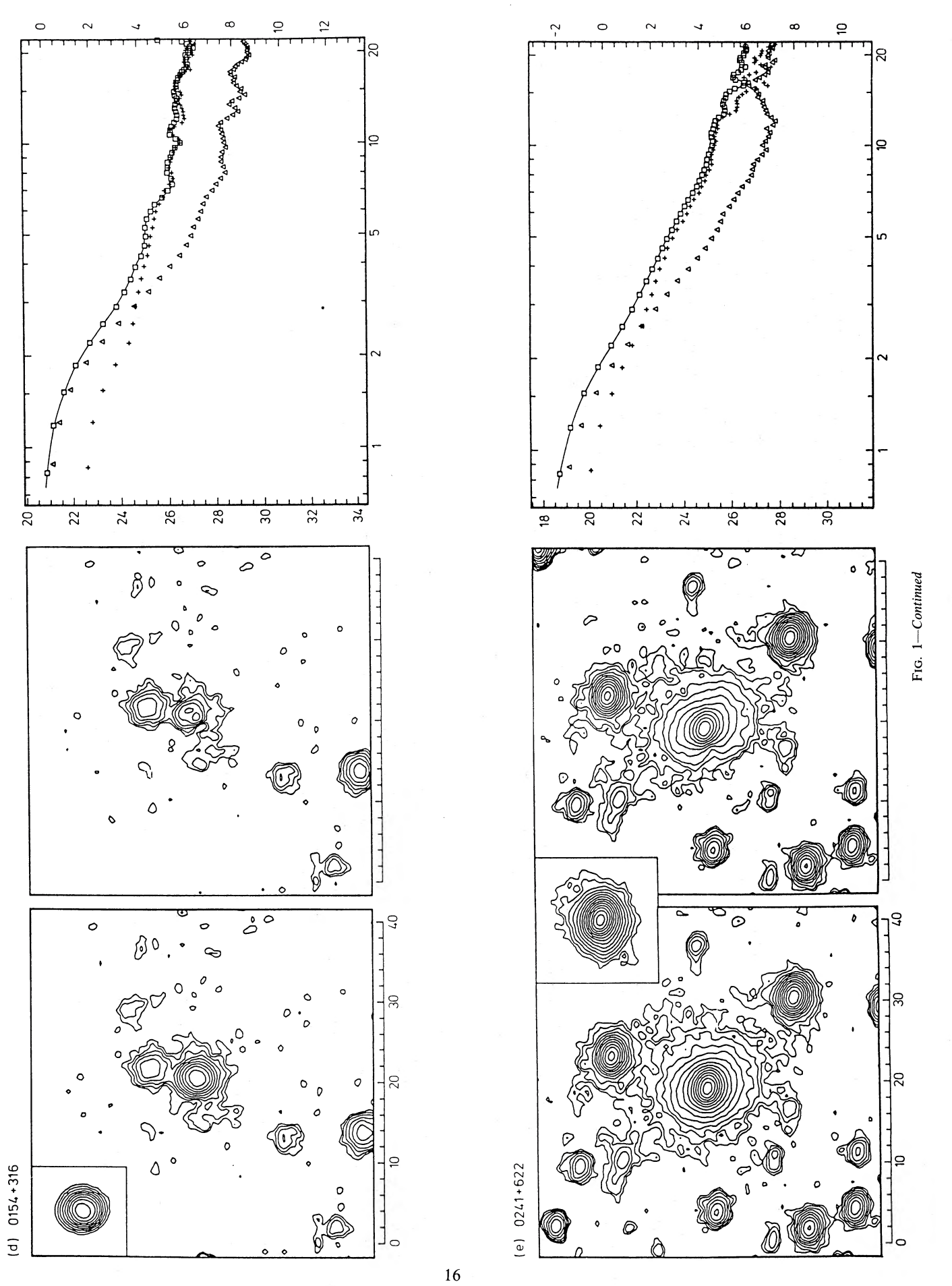
which for all program objects except 0241+622 results in extinction values of less than 0.3 mag. The quasar 0241+622 is very near the galactic plane, and we have adopted  $A_r = 3.0$  from the  $A_v = 4.6$  mag absorption derived by Margon and Kwitter (1978; cf. also Hutchings *et al.* 1982).



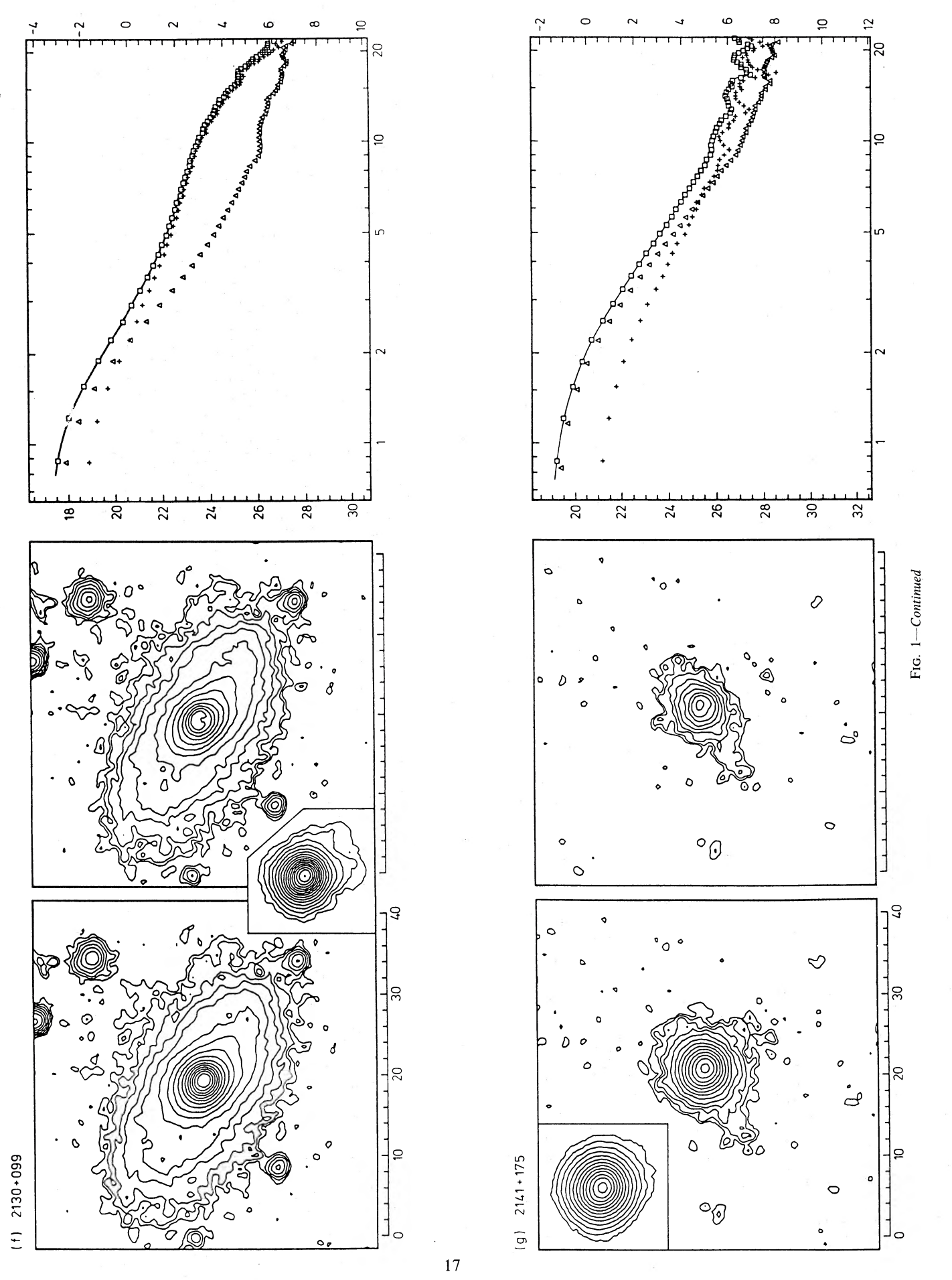
QSO. (center) Residual image of underlying galaxy produced by point-by-point subtraction of the appropriately scaled comparison star (PSF) shown in the inset. North is up, and east is to the left. Contours are spaced by 0.5 mag arcsec<sup>-2</sup> starting at 25.0 mag arcsec<sup>-2</sup>. Scale in arcsec is given below the figure on the left. (right) Azimuthally averaged intensity profiles on a double logarithmic scale. Squares, quasar; triangles, point-spread function; crosses, residual underlying galaxy. Scale on the left denotes surface brightness in the r bandpass in mag per square arcsec; scale on the right refers to surface brightness in magnitude units with respect to the red night sky. Radial distance from the center of the image in arcsec is plotted on the bottom axis. Fig. 1.—Isophotal images and azimuthally averaged intensity profiles of quasars observed with the CCD. Objects (a) to (k) are labeled by their coordinate designation. (left) Fully reduced image of the



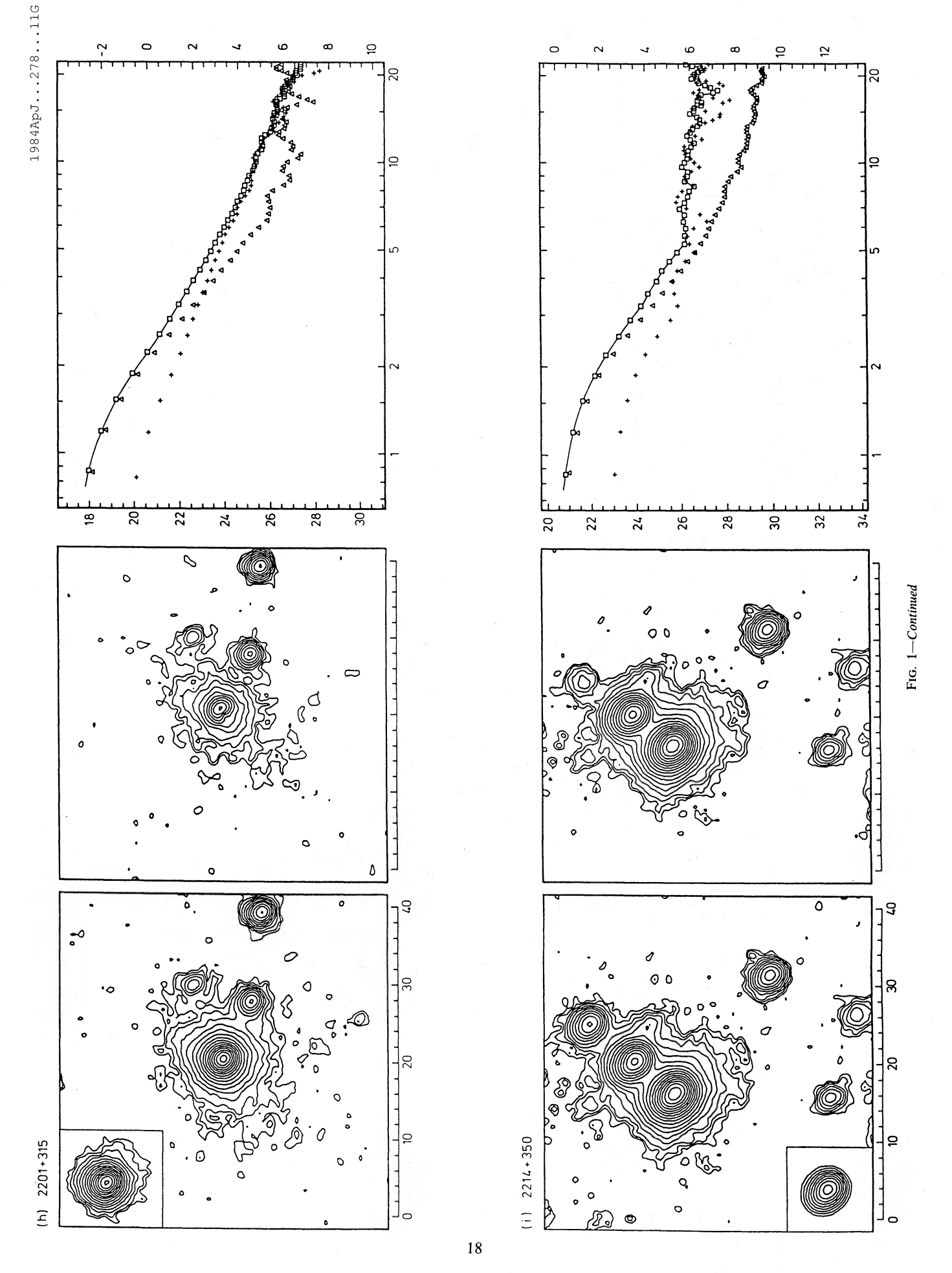
 $@ \ American \ Astronomical \ Society \ \bullet \ \ Provided \ by \ the \ NASA \ Astrophysics \ Data \ System$ 



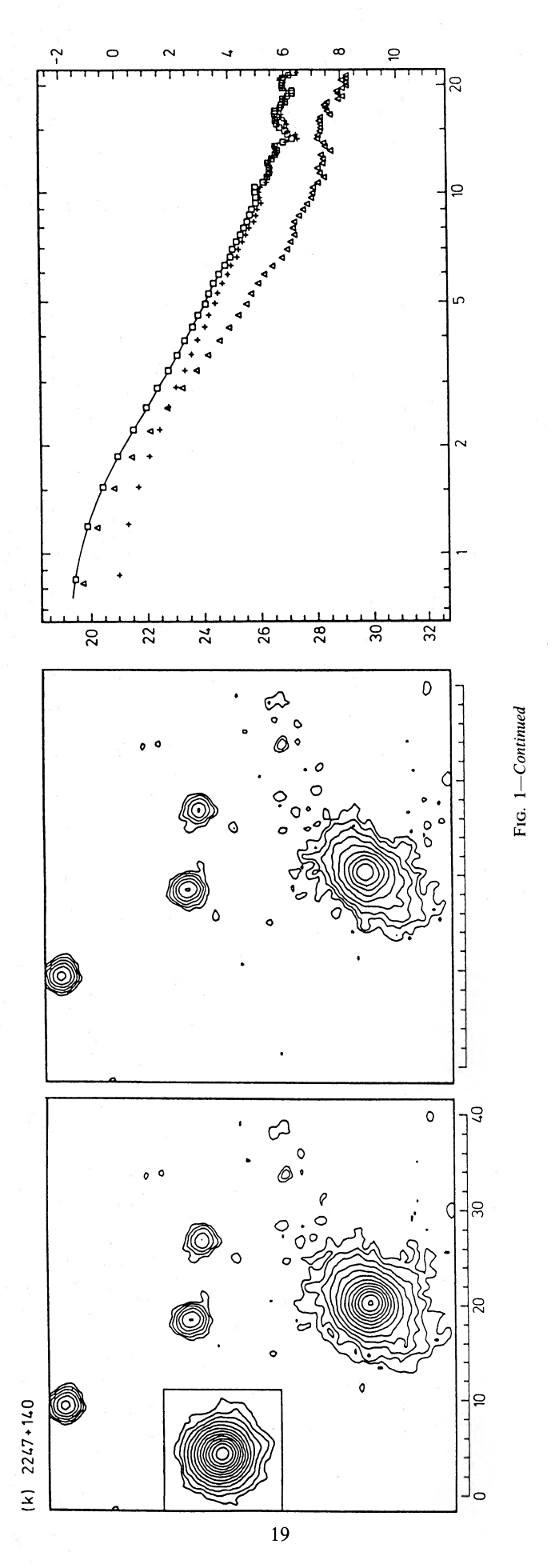
 $@ \ American \ Astronomical \ Society \quad \bullet \quad Provided \ by \ the \ NASA \ Astrophysics \ Data \ System$ 



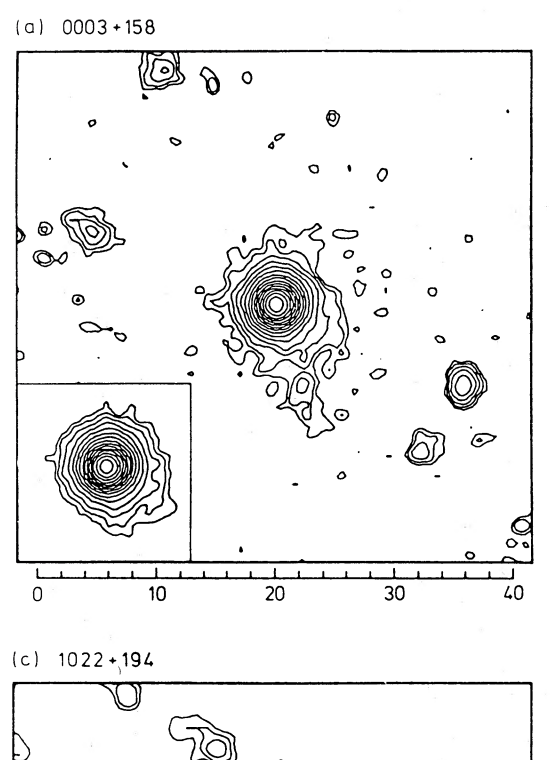
 $@ \ American \ Astronomical \ Society \ \bullet \ \ Provided \ by \ the \ NASA \ Astrophysics \ Data \ System$ 

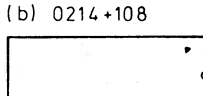


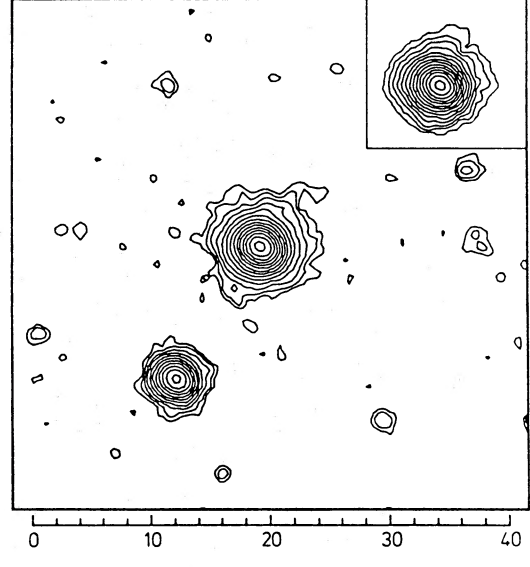
 $@ \ American \ Astronomical \ Society \ \bullet \ \ Provided \ by \ the \ NASA \ Astrophysics \ Data \ System$ 

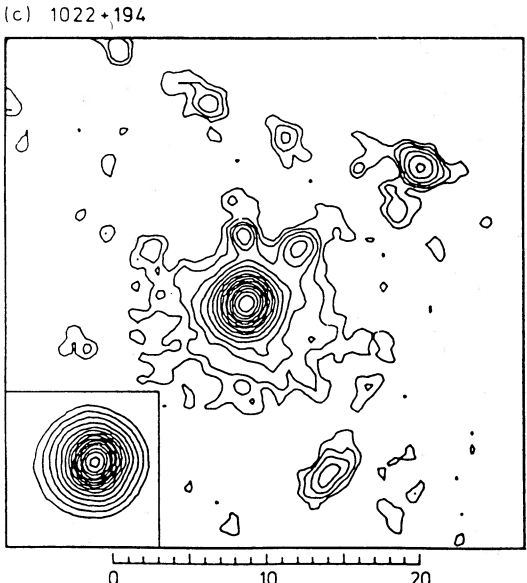


 $@ \ American \ Astronomical \ Society \ \bullet \ Provided \ by \ the \ NASA \ Astrophysics \ Data \ System$ 









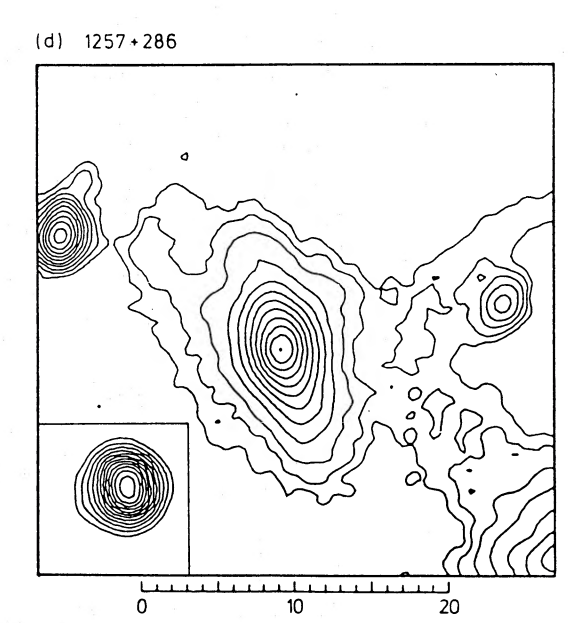
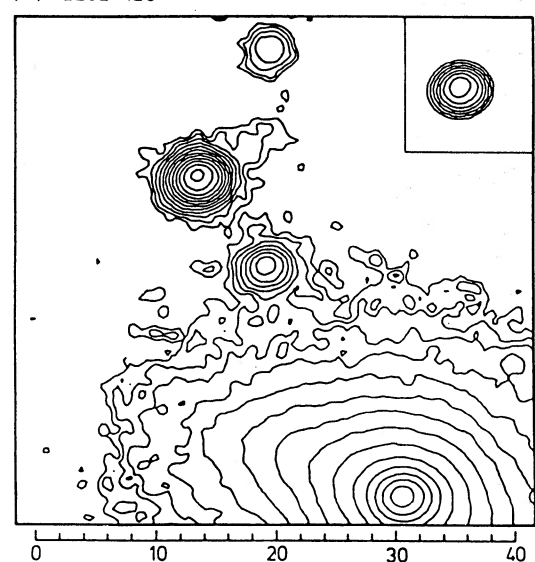


Fig. 2.—Isophotal images of quasars and comparison stars (insets) observed with the CCD. Spacing of isophotes is 0.5 mag arcsec<sup>-2</sup>, starting with 25.0 at the lowest level, except for 1022+194 and 2252+129, where the contours start with 26.0 and 24.5, respectively.

The K-corrections for the galaxies, including the spectrum shift and bandwidth terms, have been recomputed for the r bandpass and the IIIa-F/OG 570 plate-filter combination, using ultraviolet spectra of standard E galaxies obtained by Oke, Bertola, and Capaccioli (1981). The K-corrections are given in Table 3 and deviate slightly from those predicted by interpolation in Whitford's (1975) table. We note that the corrections obtained for the r and F bandpasses are very similar since both occupy approximately the same wavelength range.

No such simple approach is possible for the K-correction of the quasar nuclei. Hutchings et al. (1982) have used mean energy distribution of quasars. However, inspection of all available spectra of quasars reveals that although in general their spectral energy distributions are relatively flat, emissionline strengths (i.e., Balmer lines of Fe II multiplets) are quite different, and they may provide strong individual contributions to the K-correction. Since the K-correction thus expected for the quasar nuclei based on the spectral energy distribution of the continuum alone is relatively small, we decided to neglect the K-corrections for the quasar nuclei.

Absolute magnitudes and metric diameters of the underlying galaxies refer to a Friedmann universe with  $q_0 = +1$  and  $H_0 = 75$  km s<sup>-1</sup> Mpc<sup>-1</sup>, and are presented in columns (8) and (9) of Table 2. The luminosity ratio  $L_{\text{Nucl}}/L_{\text{Gal}}$ , reduced to rest frame r bandpass is shown in column (10), while the



(f) 2308+098

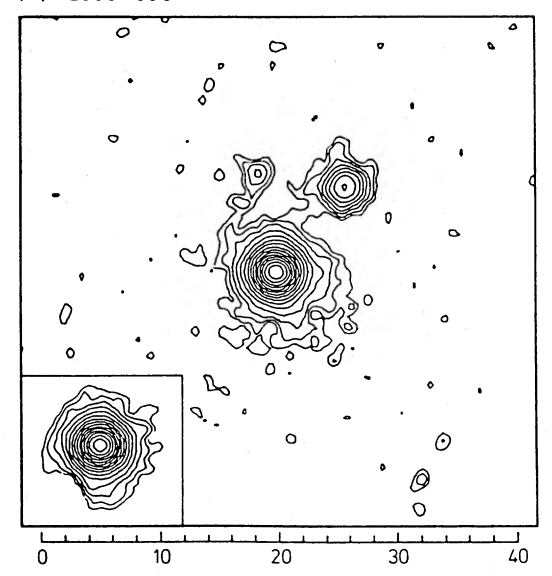


FIG. 2—Continued

last column in Table 2 contains the mean power-law exponent of the radial intensity image profile. Our data confirm that host galaxies of quasars are observed over an appreciable range of integrated absolute magnitudes and hence cannot be taken as standard candles. The mean absolute magnitude of galaxies underlying radio-loud quasars,

$$\langle M_r \rangle = -22.8 \pm 0.7$$
 (10 radio-loud quasars),

is comparable to the mean value of  $M_r = -23.0$  found for the average absolute magnitude of the brightest cluster galaxies

(Kristian, Sandage, and Westphal 1978). The mean absolute magnitude of the galaxies underlying *radio-quiet* quasars may be significantly fainter,

$$\langle M_r \rangle = -20.5 \pm 1.3$$
 (3 radio-quiet quasars),

but the sample is small and therefore may not be representative. The average metric diameter of the host galaxies of the 10 radio-loud quasars is  $\langle D \rangle = 128 \pm 34$  kpc, and  $\langle D \rangle = 37 \pm 8$  kpc is found for the three radio-quiet quasars. This difference in average metric diameters may indicate that

TABLE 2
PROPERTIES OF UNDERLYING GALAXIES

QSO (1)	Type (2)	(3)	$m_r^a$ (4)	θ <sup>b</sup> (5)	$K_r(z)$ (6)	$A_r$ (7)	M, c (8)	D <sup>d</sup> (9)	$L_{ m Nucl}/L_{ m Gal}^{ m e}$ (10)	$\alpha^{\rm f}$ (11)
1. 0003 + 158	R	0.450		< 13	0.77	0.03				
$2. \ 0043 + 388 \dots$	0	0.189	20.7:	7:	0.27	0.11	-19.1:	29:	2.4:	
3. 0054 + 144	R	0.171	17.1	25	0.23	0.03	-22.4	92	2.0	-1.91
4. 0134 + 329	R	0.367	17.3	17	0.56	0.08	-24.1	156	1.4	-2.43
5. 0154 + 316	R	0.373	19.3:	14	0.56	0.08	-22.2:	131	0.9	-1.21:
6. 0214 + 108	R	0.408	18.9	10	0.64	0.03	-22.9	106	3.7	-2.21
7. 0241 + 622	R	0.044	17.0	156 <sup>g</sup>	0.05	$3.0^{g}$	$-22.2^{g}$	$134^{g}$	1.3	-2.19
9. 1022 + 194	R	0.828		< 6	2.37:	0.02				
10. $1257 + 286 \dots$	O	0.092	17.0	20	0.11	0.00	-20.9	38	0.4	-2.06
11. 2130 + 099	O	0.061	15.5	37	0.07	0.08	-21.6	45	0.9	-2.04
12. 2141 + 175	R	0.213	17.8	16	0.31	0.10	-22.3	. 76	2.3	-2.13
13. 2201 + 315	R	0.297	17.1	25	0.45	0.17	-23.9	177	2.1	-1.95
14. 2214 + 350	R	0.510	20.2:	9:	0.99	0.19	-22.5:	140:	2.0:	
15. 2247 + 140	R	0.237	17.8	18	0.35	0.05	-22.5	97	1.2	-2.06
16. $2252 + 129 \dots$	R	0.543		10:	1.15	0.04		179:		
17. 2308 + 098	R	0.432	18.7:	10	0.71	0.03	-23.2:	116	4.9:	-1.39:

<sup>&</sup>lt;sup>a</sup> Apparent r magnitude of resolved underlying galaxy; colon denotes uncertain value.

<sup>&</sup>lt;sup>b</sup> Mean angular diameter in arcsec, at  $\mu_r = 26$  mag arcsec<sup>-2</sup>

<sup>&</sup>lt;sup>c</sup> Absolute r magnitude of underlying galaxy, assuming  $H_0 = 75$  km s<sup>-1</sup> Mpc<sup>-1</sup> and  $q_0 = +1$ , corrected for  $K_r(z)$  and galactic extinction.

<sup>&</sup>lt;sup>d</sup> Metric diameter in kpc, at  $\mu_r = 26$  mag arcsec<sup>-2</sup>.

<sup>&</sup>lt;sup>e</sup> Luminosity ratio referring to rest frame r bandpass.

f Mean intensity profile power-law exponent.

<sup>&</sup>lt;sup>g</sup> Assuming  $A_v = 4.6$  (cf. Margon and Kwitter 1978).

TABLE 3

K-Corrections for Thuan-Gunn Filters and IIIa-F + OG 570 Based on the Spectral Energy Distribution of Standard E Galaxies (Oke, Bertola, and Capaccioli 1981)

z	$K_g$	K,	$K_F$
0.0	0.00	0.00	0.00
0.1	0.32	0.12	0.14
0.2	0.89	0.29	0.31
0.3	1.51	0.46	0.49
0.4	1.93	0.62	0.73
0.5	2.30	0.94	1.13
0.6	2.73	1.42	1.62
0.7	3.27	1.91	2.12
0.8	3.78	2.31	2.40
0.9	4.25	2.53	2.69
1.0	4.60	2.81	2.97

radio-quiet quasars are found in smaller galaxies than the radio-loud quasars, since it corresponds to the bimodal distribution of absolute magnitudes. Attempts to relate the smaller diameters of host galaxies of radio-quiet quasars to inclination effects do not seem to be very promising because the observed differences in axial ratios are only marginal.

Improvements introduced into the two-dimensional CCD data reduction procedure, namely, two-dimensional point-bypoint subtraction of the scaled PSF under the constraints discussed in § II, yield substantially increased values of the central surface brightness for the underlying galaxy component compared with previously used techniques (Wyckoff, Wehinger, and Gehren 1981). Thus the data of Wyckoff et al. have been reprocessed using the same reduction procedure as for the current CCD observations. Their revised mean absolute magnitude, based on 14 radio quasars, is  $\langle M_F \rangle = -22.6 \pm 0.7$ , again for  $H_0 = 75$  km s<sup>-1</sup> Mpc<sup>-1</sup>, while the seven radio quasars listed by Hutchings *et al.* (1982) yield  $\langle M_F \rangle = -22.7 \pm 1.8$ . Since the r and F bandpasses are very similar, the extension of our data to a total of 30 radio-loud and seven radio-quiet quasars observed with either photographic emulsion or CCD but reduced with the same techniques results in a mean absolute magnitude for the host galaxies of radio quasars of  $\langle M_r \rangle = -22.5 \pm 0.8$  and a mean absolute magnitude of optically selected quasars of  $\langle M_r \rangle =$  $-21.0 \pm 1.2$ . The latter compares with  $-21.7 \pm 1.5$  derived for the radio-quiet quasars in the list of Hutchings et al. (1982).

Out of a total of 43 radio-loud quasars observed to date, 14 have not been resolved, among them two low-redshift quasars (0607-157, z=0.324 and 1203+011, z=0.104), for which upper magnitude limits of underlying galaxies are  $M_r > -18.6$  and -17.6, respectively. All other unresolved quasar host galaxies imply upper limits well in the range of absolute magnitudes reported here.

# b) Intensity Profiles

It has been found previously (Hutchings et al. 1982) that radial intensity profiles of quasar host galaxies conform to an exponential law. The new CCD data presented here seem to fit better a *Hubble law*. Inspection of the well-resolved galaxy profiles shown in Figure 1 immediately reveals the straight-

line character of these profiles in the double logarithmic diagram,  $\log I = \alpha \log r + \mathrm{const.}$  Individual values for the power-law exponent  $\alpha$  are given in Table 2. Linear least-squares fits to the profile points have been restricted to the range 1".5  $\lesssim r \lesssim 15$ " to exclude the centers of the underlying galaxies, where the data reduction procedure is unreliable (cf. § II). The outer wings were excluded because of image degradation from circular fringing or by errors in determining the sky background.

The difference between the two types of intensity laws is demonstrated in Figure 3, where the images of seven well-resolved host galaxies of quasars have been co-added to produce a mean intensity profile. Quite obviously there is no reasonable fit to an exponential intensity law in the lower panel, while the excellent straight-line fit to the data points for the seven quasar host galaxies represented in the upper panel,

$$\log I(r) = \alpha \log r + \text{const}, \quad \alpha = -2.10 + 0.17$$

corresponds to a Hubble intensity law for elliptical galaxies. The mean power-law exponent from all data, radio-loud and radio-quiet, given in Table 2 is  $\alpha = -1.96 \pm 0.36$ , where the relatively large scatter results from the host galaxies of 0154 + 316 and 2308 + 098, which are only marginally resolved. No evidence is found that the host galaxy intensity profiles of radio-quiet and radio-loud quasars follow different power laws. Since we feel that the intensity profiles provide strong evidence in favor of elliptical galaxies, we have examined in some detail effects which might invalidate our conclusions:

1. Photometric noise is negligible as far as the intensity profiles are concerned. The signal-to-noise ratio at the sky background level is greater than 35, and azimuthal averaging improves it by a factor of 6 at r = 1.5 and a factor of  $\sim 20$  at r = 1.5 (this is in fact the reason why we can reach very low surface brightnesses at all).

2. Azimuthal averaging itself does not strongly affect the run of the image profiles. Mean profiles synthesized from exponential or power-law intensity distributions for various axial ratios show that, while the scale height parameters change their values, the functional dependence of the intensity profiles remains essentially unchanged.

3. In principle the photometric accuracy of the CCD data is high enough to allow a two-dimensional deconvolution. However, it seems that there remain problems (low spatial resolution, defective pixels) which require further investigations before reliable photometric results are obtained. Meanwhile, one way to examine the influence of the point-spread function (PSF) on the host galaxy intensity profiles is to convolve exponential or Hubble-type intensity distributions with that of the PSF. Approximating the PSF by a Gaussian central component with wings extended  $\sim r^{-4}$ , as suggested by Figure 1, and assuming a broad range of seeing half-widths and scale height parameters, we find that the resulting convolution does not deviate significantly in its functional dependence from that of the original profile for r > 2''.

4. While we have emphasized the excellent fit to a power law, we note its failure to reproduce the observed profiles outside  $r \approx 15$ ", which is clearly displayed by the excess intensities in Figure 3. As is evident from the intensity profiles of single objects (e.g., Figs. 1b, 1c, 1e, 1g, 1k), this effect is mainly a result of circular fringing (cf. § II) and a

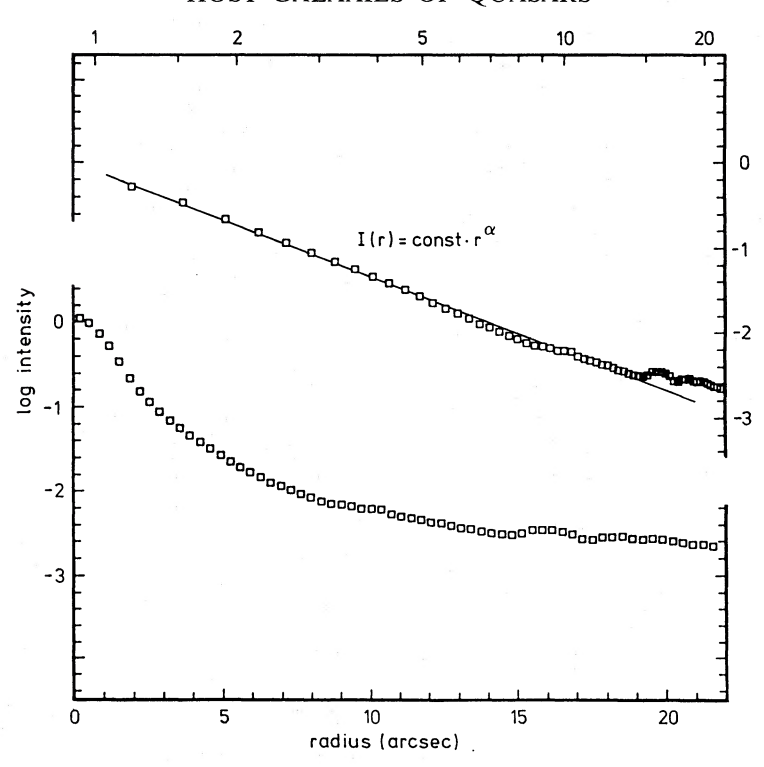


Fig. 3.—Azimuthally averaged intensity profile obtained from co-adding seven well-resolved host galaxies of quasars observed with the CCD. The same profile is plotted on a logarithmic (upper panel) and on a linear (lower panel) radius scale. The straight line shows the excellent fit to a power law with  $\alpha = -2.1$ .

correspondingly uncertain background determination. Furthermore, there may exist a contamination of the intensity profiles by very faint background objects which remain undetected but yet contribute to a flattening of the profiles.

5. For the well-resolved profiles co-added in Figure 3, our power-law fit does *not* depend crucially on the reduction procedure. Our procedure of subtracting the maximum PSF contribution resulting in a monotonically increasing difference profile appears to be the only one giving physically meaningful results. Changing to the subtraction of a *minimum* PSF contribution of course will result in no decomposition at all, and subtracting a maximum PSF contribution without restrictions for the residual profile will produce a strong central intensity dip. In either case the outer parts of the residual intensity profiles  $(r \gtrsim 5'')$  are changed in a continuous way by small amounts only. Thus for the present sample of well-resolved quasar host galaxies we find *no* evidence for intensity profiles resembling those of spiral galaxies.

# c) Luminosity Ratios

The luminosities of the QSO nuclear components and those of the resolved underlying galaxies (QSO nuclei removed) are compared in column (10) of Table 2. The ratio  $L_{\rm Nucl}/L_{\rm Gal}$  refers to the rest frame r bandpass and includes the K-correction for the host galaxy. Formally, a mean value

$$\langle L_{\text{Nucl}}/L_{\text{Gal}} \rangle = 2.0 \pm 1.2$$

is obtained for the data presented in Table 2. Figure 4 shows that the luminosities of the quasar nuclei may be loosely correlated with the absolute magnitudes of their host galaxies.

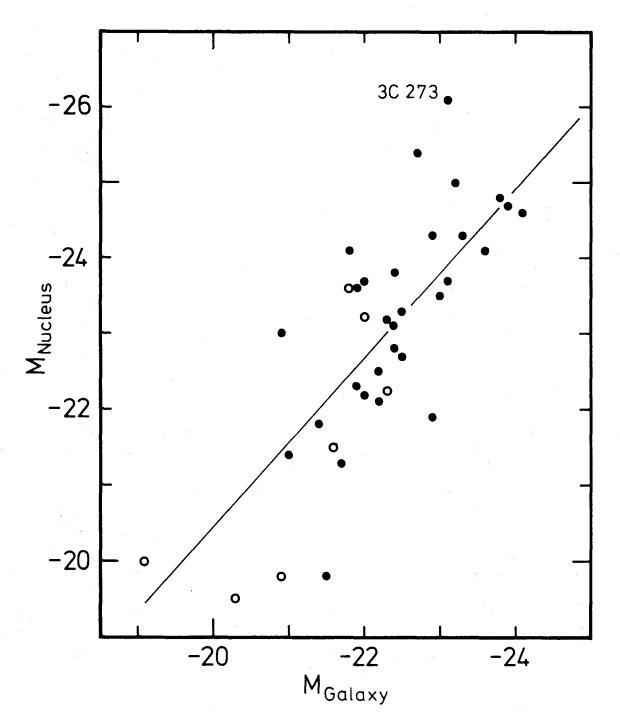


FIG. 4.—Absolute magnitudes of quasar nuclei vs. absolute magnitudes of underlying galaxies including K-correction. Data obtained from previous photographic observations refer to the F bandpass; data from current CCD observations, to the r filter. The straight line shows the linear regression,  $M_{\rm Nucl}=1.12M_{\rm Gal}+{\rm const.}$  Open and filled circles refer to optically and radio selected quasars, respectively. Magnitudes are based on a Friedmann model with  $H_0=75~{\rm km~s^{-1}~Mpc^{-1}}$  and  $q_0=+1.$ 

24

The regression line, including the data obtained previously with photographic techniques, implies

$$M_{\text{Nucl}} = 1.12 M_{\text{Gal}} + \text{const}$$
,

which is roughly compatible with a constant mean luminosity ratio. The excessive nuclear luminosities obtained for 3C 273 and PKS 1302 – 102 are based on photographic observations and should be accepted with some caution, because saturation effects may remain near the quasar image center. It should be noted that some of the currently unresolved quasars have very luminous nuclei, which indicates that the upper left of Figure 4 may not be completely empty. The lower right part of the diagram is possibly filled by very luminous galaxy types with only marginal nuclear activity, which would never have been called a QSO. Thus the observed correlation may only describe the upper limit of a continuous distribution of extremely luminous galaxies with different amounts of nuclear activity.

Our luminosity ratios  $L_{\rm Nucl}/L_{\rm Gal}$  are in discordance with those published by Hutchings *et al.* (1982) for three of the four quasars common to our lists. This is particularly surprising for the well-resolved low-redshift quasar 0241+622, for which our luminosity ratio is a factor of 3 smaller. We emphasize, however, that our luminosity ratios are derived assuming zero K-correction for the quasar nuclei (cf. § IIIa).

# d) Notes on Individual Objects

0003+158 = PHL 658: Extended structure is probably present at low light level. Jetlike extension to the south surrounds a 22nd magnitude object at 7" from the central source, which may be a companion galaxy. At least five other galaxies with  $m_r > 21$  mag are seen within a distance of 30" (Fig. 2a).

0043 + 388: Only marginally resolved due to poor guiding. The magnitudes of the galaxies 14" S and 27" NE of the QSO are 19.5 and 19.9, respectively (Fig. 1a).

 $0054 + 144 = PHL\ 909$ : The luminous material nearly bridging the gap between the host galaxy of the quasar and the 20.6 mag galaxy 15" from the QSO may indicate tidal interaction. Three other galaxies with  $m_r \ge 19.7$  are seen in the immediate vicinity of the well-resolved quasar image (Fig. 1b).

0134+329=3CR 48: Faint wisp in NW direction was originally noticed by Matthews and Sandage (1963). Our image (Fig. 1c) definitely shows an underlying galaxy with a faint extension to the NW. The 23rd magnitude object 12" to the NW of the quasar just at the outer edge of the extension could be a companion galaxy. Boroson and Oke (1982) estimate the absolute magnitude of the host galaxy of 3CR 48 to be brighter than  $M_v = -23$ . Our data yield  $M_r = -24.1$  and make it the *brightest* host galaxy of any quasar observed so far.

0154 + 316 = 4C 31.06: This quasar lies 6" south of a 19.9 mag galaxy and is surrounded by six other galaxies in the range  $19.5 < m_r < 21.5$  mag (Fig. 1d).

 $0214 + 108 = 4C \ 10.06$ : Poorly resolved (Fig. 2b).

0241+622: Listed here as a radio quasar, because weak radio emission has been observed by Tzanetakis et al. (1978). Also known as an X-ray source (Apparao et al. 1978). Hutchings et al. (1982) give a detailed discussion of this object including its puzzling high-resolution radio structure. Margon and Kwitter (1978) have found strong galactic extinction,

 $A_v=4.6$  mag. The r bandpass extinction used here,  $A_r=3.0$  mag, is based on their  $A_v$  assuming a monochromatic reddening law  $\sim \lambda^{-1}$ . Isophotal and metric diameters have been corrected for galactic extinction using the observed power law for the intensity profiles. Our data reach about 1.5 mag arcsec<sup>-2</sup> deeper than those of Hutchings  $et\ al.$ , and there are two faint bridges apparently connecting the host galaxy of the quasar with two galaxies 14" NE and 11" SE of the QSO. The indentation of the host galaxy contours to the east of the center is due to a defect in the comparison star image (Fig. 1e).

0429 + 415 = 3CR 119: Optically identified by Kristian and Sandage (1970) as a very faint object ~1."5 SW of a 19th magnitude star. Since the seeing was ~2" during our observation, the quasar image was badly contaminated by scattered light from the nearby star. No decomposition of stellar and quasar image was possible. (No isophotes shown.)

1022+194=4C 19.34: Comparison of stellar and quasar image (Fig. 2c) shows the extended faint envelope at ~26 mag arcsec<sup>-2</sup>. Yet point-by-point subtraction yields a poorly defined image. Estimated integrated magnitude of nebulosity is compatible with the high redshift of z=0.828. The underlying nebulosity seems to be heavily distorted, showing multiple extensions directed toward at least eight galaxies in the immediate vicinity.

1257 + 286 = X Comae: Faint envelope was detected by Bond (1973). Bond and Sargent (1973) have classified it as an N-type or Seyfert galaxy; however, by its luminosity ratio,  $L_{\rm Nucl}/L_{\rm Gal} = 0.4$ , X Comae may be classified as a quasar. The outermost isophotes of the underlying galaxy show a highly elongated nearly rhombic shape with a broad luminous extension to the NE (Fig. 2d).

2130+099 = II Zw 136: Previously also classified as a Seyfert galaxy. The contours resemble spiral structure. A careful examination of low light level isophotes reveals that the NE extension of the galaxy is split into at least three components. II Zw 136 is surrounded by four galaxies, ranging from 19.9 to 22.0 mag, which may be physically associated with the quasar (Fig. 1f).

2141 + 175 = OX 169. Also observed as an X-ray source (Tananbaum *et al.* 1979) with significant variability on a time scale of a few hours. The jetlike extension to the SE was observed by Hutchings *et al.* (1982) and may be a faint companion galaxy (Fig. 1g).

 $2\overline{201} + 31\overline{5} = 4C 31.63$ : Extended, very luminous host galaxy with an apparent companion galaxy of 21.1 mag 10" to the NW (Fig. 1h).

2214+350: The image of this QSO (NW component of triple in Fig. 1i) is severely degraded by scattered light from two very bright probably foreground stars. Properties of the underlying nebulosity are therefore poorly determined, as indicated by colons in Table 2.

2247 + 140 = 4C14.82: Unfortunately, this object is near the edge of the CCD frame (Fig. 1k). The underlying galaxy of this quasar shows a bent structure similar to that of 3CR 48. It is accompanied by a pair of galaxies (20.5 and 21.2 mag) approximately 20" N of the QSO. Similar observations have been published by Hutchings *et al.* (1982).

2252+129 = 3CR 455. This is one of the objects discussed by Arp et al. (1972) and Arp, Pratt, and Sulentic (1975), who claim that 3CR 455 (center, Fig. 2e) has been ejected from

the nearby galaxy NGC 7413. This faint quasar may be marginally resolved, but the outer isophotes merge with those of the extended envelope of NGC 7413. We mention that our isophotes of the QSO do *not* look starlike as was claimed by Arp *et al.* Magnitude and diameter of the underlying nebulosity estimated from our data are in agreement with the values expected for a redshift of z = 0.543.

2308 + 098 = 4C 09.72: Because of image deformation of the comparison star (Fig. 2f) subtraction of the PSF was a poor approximation to removal of the pointlike nucleus. Faint filaments appear to connect the underlying galaxy with two nearby galaxies lying 10'' to the NE and NW with apparent magnitudes  $m_r = 19.6$  and 22.0, respectively.

### IV. CLUSTERING OF GALAXIES AROUND QUASARS

In the fields of nearly all quasars observed with large-scale sky-limited techniques, numerous faint galaxies are frequently present, often with a pronounced concentration in the immediate neighborhood of the quasars. Examples can be found in Wyckoff, Wehinger, and Gehren (1981). There is now some evidence that most and perhaps all quasars are associated with groups or small clusters of galaxies (Stockton 1978, 1980). As we have already noted above, many of the quasars in our current sample observed with the CCD are not only surrounded by faint galaxies but also appear to be tidally interacting with close companions. Hutchings et al. (1981, 1982) and Hutchings and Campbell (1983) have also noted apparent interactions in their quasar studies. Although spectroscopic observations will be needed to confirm the physical association of the faint galaxies near the quasars, it may be useful to compare the apparent clustering of galaxies near quasars with what might be expected from a uniform galaxy background.

Using only our CCD data, the following difficulties are encountered: (a) Since the CCD frame covers only about  $2' \times 3'$ , only the most distant clusters are expected to be

mapped completely, and (b) because of the bright night sky, our limiting magnitude is  $m_r \approx 23.5$ , which reduces the magnitude range sampled with respect to the brightest galaxy in a cluster. However, Bahcall (1975) has found that galaxy clusters of different richness classes do not differ systematically in their core radii  $R_c$ , which, for  $H_0 = 75 \text{ km s}^{-1} \text{ Mpc}^{-1}$ , average  $\sim 150 \text{ kpc}$ . The average number of galaxies she found within this core radius was 8–19, evidently independent of the cluster richness class. On the other hand, a measure of the galaxy background density and its large-scale fluctuation can be obtained by galaxy counts over large areas of the sky. For convenience we will use the approximation provided by Tyson and Jarvis (1980),

$$\log N(m_r) = 0.41(m_r - 0.5) - 5.63, \tag{1}$$

where we have introduced a mean galaxy color index of B-r=0.50. This assumed color index influences our results only slightly, introducing a systematic correction of the same order as the differences between various galaxy counts.

The counts of galaxies in our CCD quasar fields have been restricted to the predicted core radius  $R_c = 150$  kpc. The results are presented in Table 4, where  $\theta_c$  is the angular radius in arcsec corresponding to the metric core radius  $R_c$  at redshift z. The integral numbers of galaxies counted up to a limit of  $m_r = 20$ , 21, and 22 mag are given in columns (4)–(6). The numbers in parentheses in these columns are the predicted background galaxy counts from Tyson and Jarvis's formula (eq. [1]). The photometric errors of the measured magnitudes are negligible. In column (7) of Table 4, x is the mean enhancement factor of our integral counts over the predicted background counts, where a colon indicates the less reliable data because the sampling area centered on the QSO extended across the edge of the CCD frame. In judging the significance of the local enhancement of galaxies near quasars, we note that the galaxy background is largely due to clusters apparently merged by projection effects (cf. Abell 1975), yet

TABLE 4

Counts of Galaxies within Metric Radius of 150 Kiloparsecs around Quasars

QSO (1)	(2)	$\theta_c^a$ (3)	N(20) <sup>b</sup> (4)	N(21) (5)	N(22) (6)	x° (7)	$\frac{\Delta m_r^{\rm d}}{(8)}$
1. 0003 + 158	0.450	36	0(0.07)	1(0.19)	5(0.48)	5.2	
2. 0043 + 388	0.189	58	4(0.19)	7(0.49)	7(1.25)	13.7	1.2:
3. 0054 + 144	0.171	62:	2(0.22)	7(0.56)	8(1.43)	9.2:	-2.6
4. 0134 + 329	0.367	39	0(0.09)	2(0.22)	6(0.56)	6.6	-3.3
5. 0154+316	0.373	39	2(0.09)	3(0.22)	7(0.56)	16.1	-0.6
6. $0214 + 108 \dots$	0.408	38	0(0.08)	2(0.21)	3(0.54)	5.1	-2.1
7. $0241 + 622 \dots$	0.044	192:	11(2.07)	33(5.32)	40(13.68)	4.8:	-2.4
8. 0429 + 415	0.408	38	0(0.08)	4(0.21)	10(0.54)	12.5	
11. 2130+099	0.061	143:	3(1.15)	7(2.95)	15(7.59)	2.3:	-3.6
12. 2141 + 175	0.213	53:	2(0.16)	3(0.41)	4(1.04)	8.0:	-1.6
13. 2201 + 315	0.297	44	1(0.11)	6(0.28)	10(0.72)	14.8	-2.8
14. 2214+350	0.510	35:	0(0.07)	2(0.18)	2(0.45)	5.2:	-0.2:
15. 2247 + 140	0.237	50:	0(0.14)	2(0.36)	3(0.93)	2.9:	-2.7:
16. 2252 + 129	0.543	34	0(0.06)	4(0.17)	4(0.43)	11.1	
17. 2308 + 098	0.432	37	1(0.08)	3(0.20)	4(0.51)	12.7	-0.9:

<sup>&</sup>lt;sup>a</sup> Angular radius in arcsec corresponding to  $R_c = 150$  kpc ( $H_0 = 75$  km s<sup>-1</sup> Mpc<sup>-1</sup>,  $q_0 = +1$ ); colon denotes incomplete sampling area.

<sup>&</sup>lt;sup>b</sup> Integral number of galaxies counted to  $m_r = 20-22$  mag. Values in parentheses refer to the predicted number of background galaxies (eq. [1], cf. Tyson and Jarvis 1980).

<sup>&</sup>lt;sup>c</sup> Mean ratio of observed and predicted galaxies; colon denotes lower limit.

d Magnitude difference between host galaxy of the quasar and brightest galaxy counted.

26

$$\langle m_{\rm QH} - m_{\rm BG} \rangle = \langle \Delta m_r \rangle = -1.80 \pm 1.42$$
.

within  $R_c$  yield a mean value

The most reliable values of  $\Delta m_r$  range from -2 to -3. If the quasars and galaxy clusters are physically associated, we conclude that most underlying galaxies of the quasars discussed here would dominate their respective clusters.

#### V. DISCUSSION

Although the CCD data presented here still contain substantial systematic errors, we do not expect these errors to exceed 0.5 mag except for a few poorly resolved objects. A source of systematic errors in the photographic data is the calibration of the magnitude scale, which was based on the assumption  $F_{QSO} = V_{QSO}$ . Currently, our CCD data lead to  $\langle V - r \rangle_{\rm QSO} = 0.11 \pm 0.63$ , which supports the assumed colors used in our previous paper (Wyckoff, Wehinger, and Gehren 1981). The absolute magnitude distribution of the resolved underlying galaxies of all QSOs is presented in Figure 5a, where the dashed histogram refers to host galaxies of radioquiet quasars only. The question mark on the left of Figure 5a indicates lack of information about possible low-luminosity host galaxies. A simple estimate taking into account the upper magnitude limits of unresolved objects could imply 5%-10% of all quasars reside in host galaxies of low luminosity  $(M_r > -19)$ . The distribution of luminosity ratios  $L_{\text{Nucl}}/L_{\text{Gal}}$  is shown in Figure 5b. Again due to our present limitations in detecting faint light levels near the sky background, we estimate that at least 10%-20% of all quasars may have  $L_{\text{Nucl}}/L_{\text{Gal}} > 10$ . As yet there appears to be no evidence that either the luminosity ratio  $L_{
m Nucl}/L_{
m Gal}$  or the luminosity of the host galaxy varies with redshift.

We tentatively classify the host galaxies of the radio quasars as giant elliptical galaxies based on the luminosities, diameters, and intensity profiles. The power-law dependence of the quasar galaxy intensity profiles found in § IIIb may indicate that most radio quasars are situated in giant elliptical galaxies. Moreover, the sizes and luminosities of the host galaxies of radio quasars are comparable to those of first-ranked cluster galaxies, though with a larger scatter in luminosities. Our data also indicate that a few radio-loud quasars as well as most of the radio-quiet QSOs appear to be associated with less luminous types of galaxies. The majority of the quasar nuclei have luminosities comparable to or slightly greater than their host galaxies. The absolute magnitudes and metric diameters of the host galaxies are consistent with the assumption that quasars are at cosmological distances.

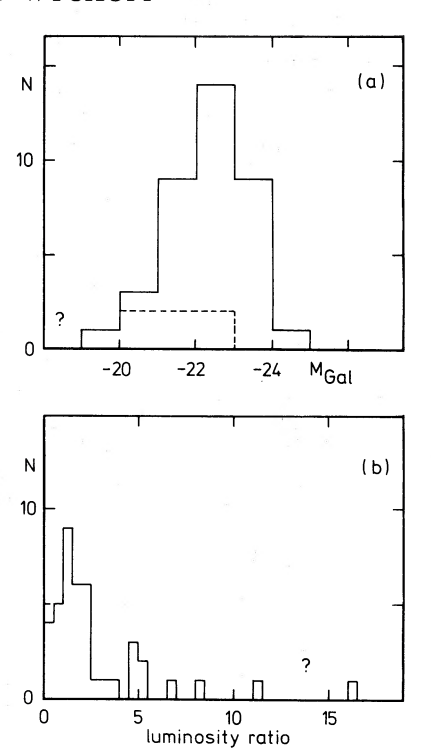


Fig. 5.—Distribution of absolute magnitudes of QSO host galaxies and luminosity ratios  $L_{\rm Nucl}/L_{\rm Gal}$ .

We note that the observed host galaxy luminosities we have derived for radio-loud and radio-quiet quasars are consistent with the luminosities derived from the spectroscopy of Boroson and Oke (1982) and Boroson, Oke, and Green (1982). Hot gas must be present in the host galaxies of radio quasars, as is evident from the narrow emission lines (cf. Wyckoff et al. 1980a; Boroson, Oke, and Green 1982). The failure to detect common absorption features of elliptical galaxies (Mg I b, Na 1 D) and the existence of Balmer-line absorption in 3CR 48 (Boroson and Oke 1982) also give evidence for a type of galaxy substantially different from normal giant elliptical galaxies. Boroson and Oke conclude that the host galaxy of 3CR 48 is a giant spiral galaxy with a 2 mag excess due to a recent burst of star formation. Even then the underlying galaxy would be exceptionally bright for a spiral. It is premature to speculate further concerning the morphologies of galaxies underlying quasars in the absence of images with high spatial resolution.

Larson and Tinsley (1978) have computed *UBV* colors of normal and peculiar galaxies assuming various modes of star formation. They also introduced bursts of star formation on time scales of 10<sup>7</sup>–10<sup>9</sup> yr, and they were able to show that very rapid bursts may be associated with peculiar objects that are *tidally distorted*. They conclude that this violent burst mode may have been particularly important during the formation of elliptical galaxies. Consequently, if violent interactions were common occurrences among the host galaxies of quasars and surrounding companion galaxies, one might expect that the large amounts of gas and early-type stars required to account for the observed spectra (Boroson and Oke 1982) are a result of close encounters or direct

collisions. Inspection of the morphological details in our observations and elsewhere (Figs. 1 and 2; see also Wyckoff, Wehinger, and Gehren 1981, Hutchings et al. 1981, 1982; Hutchings and Campbell 1983) suggests that the majority of the quasar host galaxies are tidally interacting with one or more companion galaxies. It will therefore be extremely important to investigate spectroscopically the cluster memberships of quasars, since some of the candidate companion galaxies are situated within a QSO host galaxy diameter of the QSO.

We gratefully acknowledge the support of Dr. K. Marien and W. Rauh with the instrument, and of the National Science Foundation for a travel grant for one of us (P. A. W.).

#### REFERENCES

Abell, G. O. 1975, in Stars and Stellar Systems, Vol. 9, Galaxies and the Universe, ed. A. R. Sandage, M. Sandage, and J. Kristian (Chicago: University of Chicago Press), p. 601.
Apparao, K. M. V., Bignami, G. F., Maraschi, L., Helmken, H., Margon, B., Hjellming, R., Bradt, H. V., and Dower, R. G. 1978, Nature, 273, 450.
Arp, H. C. 1970, Ap. J., 162, 811.
Arp, H., Burbidge, E. M., Mackay, C. D., and Strittmatter, P. A. 1972, Ap. J. (Letters), 171, L41.
Arp, H., Pratt, N. M., and Sulentic, J. W. 1975, Ap. J., 199, 565.
Bahcall, N. A. 1975, Ap. J., 198, 249.
Bond, H. E. 1973, Ap. J. (Letters), 181, L23.
Bond, H. E., and Sargent, W. L. W. 1973, Ap. J. (Letters), 185, L109.
Boroson, T. A., and Oke, J. B., 1982, Nature, 296, 397.
Boroson, T. A., Oke, J. B., and Green, R. F. 1982, Ap. J., 263, 32.
Gunn, J. E. 1971, Ap. J. (Letters), 164, L113.
Hawkins, M. R. S. 1978, M.N.R.A.S., 182, 361.
Hewitt, A., and Burbidge, G. 1980, Ap. J. Suppl., 43, 57. Hewitt, A., and Burbidge, G. 1980, Ap. J. Suppl., 43, 57. Hutchings, J. B., and Campbell, B. 1983, Nature, 303, 584 Hutchings, J. B., Crampton, D., Campbell, B., Gower, A. C., and Morris, S. C. 1982, Ap. J., 262, 48 Hutchings, J. B., Crampton, D., Campbell, B., and Pritchet, C. 1981, Ap. J., 247, 743. 247, 743. Kristian, J. 1973, Ap. J. (Letters), 179, L61. Kristian, J., and Sandage, A. 1970, Ap. J., 162, 391. Kristian, J., Sandage, A., and Westphal, J. A. 1978, Ap. J., 221, 383. Larson, R. B., and Tinsley, B. M. 1978, Ap. J., 219, 46. Margon, B., and Kwitter, K. B. 1978, Ap. J. (Letters), 224, L43. Matthews, T. A., and Sandage, A. R. 1963, Ap. J., 138, 30. Miller, J. S. 1981, Pub. A.S.P., 93, 681.

Miller, J. S., French, H. B., and Hawley, S. A. 1980, in *IAU Symposium 92*, Objects of High Redshift, ed. G. O. Abell and P. J. E. Peebles (Dordrecht: Objects of High Redshift, ed. G. O. Abell and P. J. E. Peebles (Dordrecht: Reidel), p. 83.

Oke, J. B. Bertola, F., and Capaccioli, M. 1981, Ap. J., 243, 453.
Richstone, D. O., and Oke, J. B. 1977, Ap. J., 213, 8.

Sandage, A., and Visvanathan, N. 1978, Ap. J., 223, 707.

Stockton, A. 1976, Ap. J. (Letters), 205, L113.

——. 1978, Ap. J., 223, 747.

——. 1980, in IAU Symposium 92, Objects of High Redshift, ed. G. O. Abell and P. J. E. Peebles (Dordrecht: Reidel), p. 89.

Tananbaum, H., et al. 1979, Ap. J. (Letters), 234, L9.

Thuan, T. X., and Gunn, J. E. 1976, Pub. A.S.P., 88, 543.

Tyson, J. A., and Jarvis, J. F. 1980, in IAU Symposium 92, Objects of High Redshift, ed. G. O. Abell and P. J. E. Peebles (Dordrecht: Reidel), p. 1. Redshift, ed. G. O. Abell and P. J. E. Peebles (Dordrecht: Reidel), p. 1.

Tzanetakis, A., Spencer, R. E., Masseu, C. R., and Baldwin, J. E. 1978, M.N.R.A.S., 185, 63.Wampler, E. J., Robinson, L. B., Burbidge, E. M., and Baldwin, J. A. 1975,

Ap. J. (Letters), 198, L49. Wehinger, P. A., Gehren, T., and Wyckoff, S. 1980, in ESO Workshop on

Two-Dimensional Photometry, ed. P. Crane and K. Kjär (Geneva: ESO),

wnittord, A. E. 1975, in Stars and Stellar Systems, Vol. 9, Galaxies and the Universe, ed. A. R. Sandage, M. Sandage, and J. Kristian (Chicago: University of Chicago Press), p. 159.
Wyckoff, S., Wehinger, P. A., and Gehren, T. 1981, Ap. J., 247, 750.
Wyckoff, S., Wehinger, P. A., Gehren, T., Morton, D., Boksenberg, A., and Albrecht, R. 1980a, Ap. J. (Letters), 242, L59.
Wyckoff, S., Wehinger, P. A., Spinrad, H., and Boksenberg, A. 1980b, Ap. J., 240, 25.

- J. FRIED: Max-Planck-Institut für Astronomie, Königstuhl, D-6900 Heidelberg, West Germany
- T. GEHREN: Universitäts-Sternwarte, Scheinerstr. 1, D-8000 München 80, West Germany
- P. A. Wehinger and S. Wyckoff: Department of Physics, Arizona State University, Tempe, AZ 85281